

PUBLISHED VERSION

Gar-Wing Truong, Eric F. May, Thomas M. Stace, and Andre N. Luiten
Quantitative atomic spectroscopy for primary thermometry
Physical Review A, 2011; 83(3):033805-1-033805-9

© 2011 American Physical Society

Originally published by American Physical Society at:
<http://dx.doi.org/10.1103/PhysRevA.83.033805>

PERMISSIONS

<http://publish.aps.org/authors/transfer-of-copyright-agreement>

Permission 4.11.2015

“The author(s), and in the case of a Work Made For Hire, as defined in the U.S. Copyright Act, 17 U.S.C. §101, the employer named [below], shall have the following rights (the “Author Rights”):

3. The right to use all or part of the Article, including the APS-prepared version without revision or modification, on the author(s)’ web home page or employer’s website and to make copies of all or part of the Article, including the APS-prepared version without revision or modification, for the author(s)’ and/or the employer’s use for educational or research purposes.”

11 October 2016

<http://hdl.handle.net/2440/88432>

Quantitative atomic spectroscopy for primary thermometryGar-Wing Truong,^{1,*} Eric F. May,² Thomas M. Stace,³ and André N. Luiten¹¹*Frequency Standards and Metrology Research Group, School of Physics, The University of Western Australia, Perth, Western Australia 6009, Australia*²*Centre for Energy, School of Mechanical and Chemical Engineering, The University of Western Australia, Perth, Western Australia 6009, Australia*³*School of Mathematics and Physics, University of Queensland, Brisbane, Queensland 4072, Australia*

(Received 20 August 2010; published 7 March 2011)

Quantitative spectroscopy has been used to measure accurately the Doppler broadening of atomic transitions in ⁸⁵Rb vapor. By using a conventional platinum resistance thermometer and the Doppler thermometry technique, we were able to determine k_B with a relative uncertainty of 4.1×10^{-4} and with a deviation of 2.7×10^{-4} from the expected value. Our experiment, using an effusive vapor, departs significantly from other Doppler-broadened thermometry (DBT) techniques, which rely on weakly absorbing molecules in a diffusive regime. In these circumstances, very different systematic effects such as magnetic sensitivity and optical pumping are dominant. Using the model developed recently by Stace and Luiten, we estimate the perturbation due to optical pumping of the measured k_B value was less than 4×10^{-6} . The effects of optical pumping on atomic and molecular DBT experiments is mapped over a wide range of beam size and saturation intensity, indicating possible avenues for improvement. We also compare the line-broadening mechanisms, windows of operation and detection limits of some recent DBT experiments.

DOI: [10.1103/PhysRevA.83.033805](https://doi.org/10.1103/PhysRevA.83.033805)

PACS number(s): 42.62.Fi, 71.20.Dg, 06.20.F-, 07.20.Dt

I. INTRODUCTION

An ability to measure absolute thermodynamic temperature is currently confined to an exclusive list of national standards laboratories. Such measurements require primary thermometry expertise and highly specialized equipment, making it impractical for wider-scale use. Instead, for practical purposes, temperature scales such as ITS-90 [1] are used as an approximation to the true thermodynamic temperature, even though they are known to have relative uncertainties at the 10^{-4} level [2]. Accordingly, there is now a global push to develop more convenient methods of primary thermometry that could make thermodynamic temperature measurements more broadly available [3]. A second motivating factor driving recent renewed interest in primary thermometry is the call by the Bureau des Internationale de Poids et Mesures to remeasure the Boltzmann constant, k_B , using a wide range of techniques in preparation for the redefinition of the kelvin in 2011 [4,5].

At present, the recommended value for k_B is derived primarily from one acoustic measurement performed by Moldover *et al.* [6]. It would be preferable if k_B could be remeasured using different methods with comparable uncertainties so that any systematic errors can be identified. Recently, Bordé suggested that the known [7] temperature dependence of the spectral linewidth of absorption features, previously exploited for measurements of stellar atmospheric temperatures [8], can be used as a new technique for accurate primary thermometry [9]. This Doppler-broadening thermometry (DBT) method has since been experimentally realized and while currently less precise than other primary methods such as acoustic or dielectric constant gas thermometry, it suffers

from very different types of systematic errors [10]. In contrast to those techniques which measure the macroscopic quantity RT , the DBT method can directly probe the microscopic thermal energy $k_B T$ by measuring the characteristic spectral width of molecular-atomic transitions, thereby avoiding the uncertainties in the Avogadro constant N_A .

The first DBT measurements performed by Daussy *et al.* and Casa *et al.* have used molecular gases at 1–130 Pa and determined k_B with a relative uncertainty [11–13] of order 10^{-4} . More recent work has improved the statistical uncertainty [14] to 4×10^{-5} . In this paper, we present results from an atomic rubidium (Rb) DBT system at 3×10^{-5} Pa. The use of an alkali-metal atom absorber presents some distinct spectroscopic differences that allow us to explore new experimental regimes within the DBT method. In doing so, we have identified some advantages in using an atomic system and encountered new challenges whose resolutions demand a deep understanding and detailed unification of light-matter interactions and gas dynamical theories [15]. While this work has been motivated by primary thermometry, we believe that it has wider implications in all fields requiring high-resolution or precision quantitative spectroscopy.

The primary difference between a low-pressure atomic vapor system, like Rb, and molecular experiments is that atomic motion is effusive, so collisions are extremely rare. An advantage of moving to this effusive regime is the avoidance of pressure-induced systematic changes, such as collisional line-shape perturbations [16]. This removes the need to extrapolate results to an equivalent zero-pressure value. Further, by using a sealed vapor-pressure reference gas cell, we avoid any unintended pressure drifts associated with a more sophisticated variable-pressure gas chamber. In this study, we chose Rb, which has a high optical cross section, ensuring that the absorption signal-to-noise ratio is satisfactory in spite of the very low vapor density. This choice also gives the ability

*Gar-Wing.Truong@physics.uwa.edu.au

to operate in a range where high-quality lasers are readily available and where silicon detectors, with their extremely good linearity [17] and quantum efficiency, can be used. At room temperature, it was possible to use a smaller cell than those in the molecular experiments for the same absorption depth, which was convenient for thermal control.

On the other hand, there are also disadvantages to using atomic vapors. Care is required to ensure low levels of residual magnetic fields which can lead to the broadening of spectral lines by lifting the degeneracy of Zeeman levels. In the transition used in this experiment (D_2 line of ^{85}Rb), optical pumping between unresolved hyperfine transitions contributed the greatest potential for systematic error by perturbing the line shape. In addition, the comparability of the natural lifetime, beam transit time, and the Rabi period in our situation leads to optical pumping effects that requires either an accurate model of the gas kinetics [15] or the use of a low-power probe beam to avoid line-shape perturbations. We followed the second route here and show here that the resulting perturbation is at the 4 ppm level. We note, however, that it should be possible to operate at higher power levels and use the model of Stace and Luiten [15] to correct the results.

The remainder of this paper is organized as follows. In Sec. II, we describe the experimental setup and data acquisition for a Rb DBT experiment. The theoretical absorption coefficient line shape for unperturbed atoms and the derivation of a suitable line-shape profile for extracting the quantity $k_B T$ from the acquired spectra are then described in Sec. III. Our experimental results are presented in Sec. IV, followed by a discussion about systematic uncertainties in Sec. V. In Sec. VI, we discuss the relative merits and challenges of the atomic approach in more detail. We also discuss how the use of atomic vapors might be extended to a wider temperature range.

II. METHOD AND EXPERIMENT

A schematic of the experimental setup used in this work is shown in Fig. 1. The $k_B T$ product was determined from

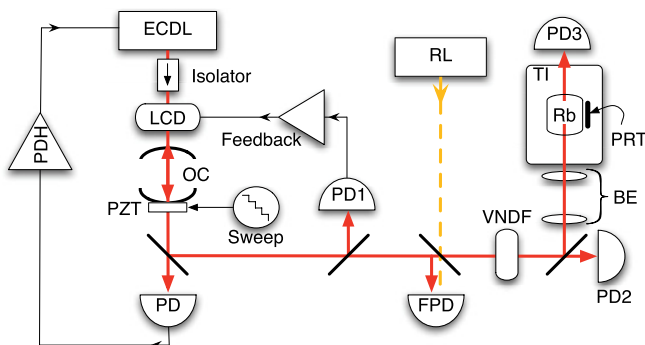


FIG. 1. (Color online) A schematic diagram of the optical circuit and electronic control systems. ECDL, extended-cavity diode laser; LCD, variable optical depth liquid crystal display; OC, optical cavity; PZT, annular piezo-electric stack; PDH, Pound-Drever-Hall top-of-resonance feedback control loop; RL, reference laser; VANDF, variable neutral density filter; BE, beam expander lenses; PRT, ITS-90 calibrated platinum resistance thermometer; TI, thermal isolator; (F)PD, (fast) photodetector.

spectroscopic measurements of unresolved hyperfine transitions (from the $5^2S_{1/2}$, $F = 2 \rightarrow 5^2P_{3/2}$, $F = 1, 2, 3$ states) in the D_2 line of ^{85}Rb at 780 nm. A custom-built extended-cavity diode laser (ECDL) was locked to a tunable optical Fabry-Perot cavity (OC) using the Pound-Drever-Hall (PDH) technique [18], which suppressed acoustic and other fluctuations of the laser frequency. We tuned the laser's wavelength by changing the length of the cavity. A sweep generator (Sweep) was used to displace one of the OC cavity mirrors by driving a piezo-electric stack actuator (PZT). A stepwise sweep was used to reduce the asynchronicity between measurements of the temperature, frequency, and absorbed power. A liquid crystal display (LCD) variable optical attenuator was used to keep the intensity transmitted through the cavity, which was monitored by the photodetector PD1, at a constant. This suppressed variations in the amount of optical pumping associated with power changes occurring throughout the scan.

The optical frequency difference between the probe and a reference laser (RL) was measured using a fast photodetector (FPD) and a high-bandwidth counter. The reference beam was derived from a tunable Ti:sapphire laser locked to a temperature-controlled, ultralow-expansion optical cavity. The stability of the RL (~ 1 kHz) contributed negligible uncertainty to the optical frequency measurement. A variable neutral density filter (VANDF) allowed measurements to be made at incident probe powers below that set by the LCD intensity control system, without affecting intensity or frequency stabilities. A photodetector (PD2) located just before the absorption cell was used to correct for any residual probe power changes. A beam expander (BE) was used to give the largest beam possible through the cell (2 cm in diameter) to maximize the input power for a given intensity to achieve a high signal-to-noise ratio. The power transmitted through a 10-cm-long Rb absorption cell was measured on a third photodetector (PD3). The Rb cell was encased in a passive thermal isolator (TI) whose temperature was monitored using a platinum resistance thermometer (PRT) calibrated to ITS-90 with 30 mK uncertainty. The maximum temperature difference across the isolator was measured to be less than 7 mK using auxiliary thermometers (not shown). The thermal relaxation time constant of the isolator (~ 2 h) was much larger than the time required for a single sweep (10 min).

The outputs of PD2 and PD3 that monitored the incident probe and the transmitted powers, respectively, were recorded using digital multimeters with five-digit resolution. A third multimeter was used to make four-wire resistance measurements of the PRT. A computer-based data-acquisition system centrally controlled and logged the three digital multimeters and the high-bandwidth counter outputs. Before each set of measurements at a fixed probe power level, the dc voltages on PD2 and PD3 caused by stray lights were recorded in the absence of the probe beam. These backgrounds were removed from the detector readings before reconstructing the Doppler-broadened absorption spectrum by dividing the output of PD3 by that of PD2.

III. EXTRACTING $k_B T$ FROM SPECTRA

In a low-density-gas cell, the absorption coefficient of an isolated spectral line is the convolution between a Lorentzian

and a Gaussian function, known as a Voigt profile [7]. The Lorentzian component can be written as $L(\nu) = \{1 + [(\nu - \nu_0)/\Gamma]^2\}^{-1}$, where ν is the optical frequency and ν_0 is the atomic transition frequency. This component arises from the finite lifetime of the upper state and has a full width at half maximum (FWHM) of $\Gamma = 1/(2\pi\tau)$, where τ is the total upper-state lifetime. Various phenomena including collisional, transit time, and power broadening can perturb the width of this Lorentzian. It was important in this experiment to keep these perturbations at negligible levels.

The Gaussian component has the form of $G(\nu) = \exp\{-[(\nu - \nu_0)/\Delta\nu_D]^2\}$, where the $1/e$ half-width of the Gaussian component is related to the thermal energy $k_B T$ as

$$k_B T = \frac{mc^2}{2} \left(\frac{\Delta\nu_D}{\nu_0} \right)^2 \quad (1)$$

and arises from the thermal motion of the atoms. Here c is the speed of light, m is the mass of the absorbing atom, and ν_0 is the absolute transition frequency. For Rb, the latter two parameters are known with relative uncertainties of 5×10^{-8} and 5×10^{-11} , respectively [19,20], which are negligible for this experiment. While it was possible to compute the absorption coefficient $V(\nu, \Delta\nu_D) = L(\nu) \otimes G(\nu)$ by performing a convolution integral, this was a computationally inefficient procedure. Instead, a numerical routine described by Humlicek [21] implemented in the scientific data analysis program IGOR PRO¹ was used to generate the Voigt function. The relative accuracy of this algorithm was better than 3×10^{-5} and no consideration of these numerical errors was required in the following analysis.

The observed transmission spectrum was determined by Beer's Law [7], $T(\nu) = \exp[-V(\nu, \Delta\nu_D)L]$, where L is the optical path length of the probe inside the absorbing gas. Since this experiment concerns frequency differences, it was convenient to shift the frequency origin by subtracting away the absolute optical frequency of the ^{87}Rb $F = 2 \rightarrow 1$ hyperfine transition. We denote these frequency differences with f to avoid confusion with the absolute frequencies ν . We performed least-squares regression of the transmission spectra to Eq. (2) to determine $\Delta\nu_D$:

$$T(f) = Af + B \exp \left(-C \sum_{i=1}^3 S_i V_i(f - f_i - f_{\text{cav}}, \Delta\nu_D) \right). \quad (2)$$

Here $T(f)$ is the sum of three unresolved hyperfine transitions, indicated schematically in Fig. 2; the $V_i(f - f_i - f_{\text{cav}})$ are the Voigt functions corresponding to each hyperfine transition, each centered on frequency f_i and with relative strength S_i ; and A , B , and C are three of the five parameters adjusted in the regression. The S_i were fixed at values derived from the Clebsch-Gordan coefficients, while the f_i were fixed at values determined by Arimondo *et al.* [20] (see Table I). Of the adjustable parameters, A and B account for, respectively, a residual background and imperfect background normalization

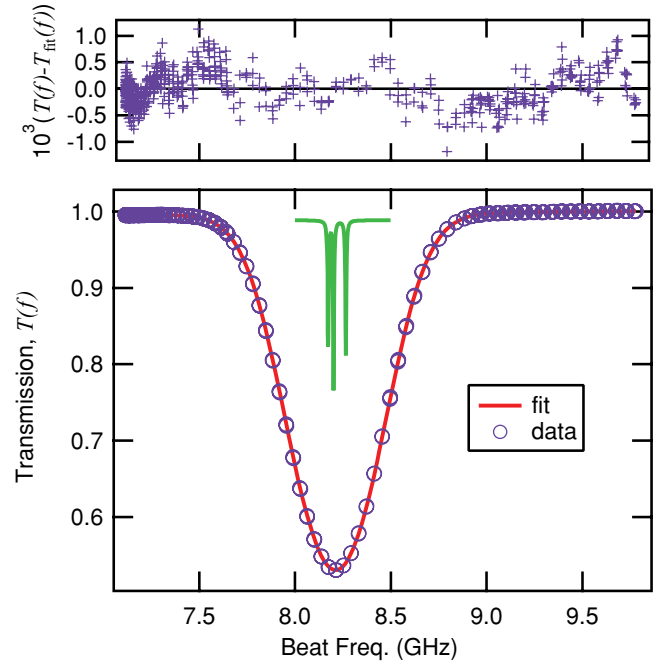


FIG. 2. (Color online) (Bottom) A typical spectrum (blue circles) obtained from Rb vapor at 295 K (~ 550 points) and the fit (red line) using Eq. (2). The Lorentzians (green) indicate both the location of the underlying hyperfine transitions and their relative strengths (in arbitrary units). (Top) The residuals to the fit.

(to a value of 1) of the spectra. C is the on resonance absorption depth determined by the number density and the cell length. The two other adjustable parameters, f_{cav} and $\Delta\nu_D$ were contained within, and were common to the three Voigt functions, with f_{cav} allowing for the arbitrary (but fixed) frequency offset of the RL from the lowest frequency hyperfine line. The Boltzmann constant was obtained from the Gaussian width $\Delta\nu_D$ using Eq. (1).

In principle, it is possible to perform the regression allowing every parameter in Eq. (2) to be adjustable. However, in this case, the returned parameters from the least-squares fit show strong correlations between a number of the free parameters. This leads a larger uncertainty range in those parameters. In particular, we find strong correlations in the S_i , and also in Γ and $\Delta\nu_D$, which have a correlation coefficient of -0.96 . Operating in an intensity range where it is possible to fix the Lorentz width and the strengths S_i to known values, we avoid an artificial inflation of the uncertainties associated with the

TABLE I. Values of the fixed constants used in Eq. (2) for the relative transition strengths, S_i , and their frequency offsets [20], f_i . The relative transition strengths are exact numbers, while there is a relative uncertainty of order 1×10^{-5} associated with the differences between the hyperfine transition frequencies.

$F_{\text{upper}} = i$	S_i	f_i (MHz)
1	1/3	4372.399(85)
2	35/81	4401.771(37)
3	28/81	4465.172(53)

¹IGOR PRO version 5.0.4.8 Wavemetrics, Inc., Portland, OR, USA.

fitted Doppler width due to these correlations. Our theoretical model (see Sec. V) guides us on the upper intensity.

IV. RESULTS

The results from several k_B determinations are shown in Fig. 4 as a function of incident probe power. These data were produced from 24 spectra taken at intensities at least 500-fold below the saturation intensity [22] ($I_{\text{sat}} \sim 20 \text{ W/m}^2$). The total uncertainties at each power level are indicated by the error bars and were determined from the standard deviation of the data sets taken at the same power level. Our final determination of the Boltzmann constant, based on a weighted mean of the measurements at the various probe powers, is

$$k_B = 1.381\,04(59) \times 10^{-23} \text{ J/K.}$$

The uncertainty in this measurement was limited primarily by residual amplitude noise at frequencies higher than the bandwidth of the LCD feedback control loop. This white noise was exacerbated by a lower-than-expected common-mode rejection of amplitude noise resulting from some asynchronicity in the data-acquisition scheme.

The broadening of the Lorentzian linewidth by magnetic fields contributed a smaller systematic uncertainty of 9.8×10^{-5} , which was summed in quadrature to give a total relative uncertainty of 4.1×10^{-4} . All other systematic uncertainties were kept at negligible levels and are discussed in the following section. However, as the random uncertainties and measurement timing are addressed in future work, these will become increasingly important. Our value of k_B has a relative deviation of 2.7×10^{-4} from the current CODATA value. To our knowledge, this is the most accurate demonstration of primary thermometry using spectroscopy of atomic absorbers.

V. ESTIMATION OF SYSTEMATIC UNCERTAINTIES

The greatest source of systematic uncertainty in this experiment was caused by Earth's magnetic field. This external field lifted the frequency degeneracy of the Zeeman sublevels in the Rb hyperfine transitions. The field along the cell was measured to be 0.21(1) G and numerical simulations show that this causes an apparent broadening of the Lorentzian linewidth by 0.5%, which in turn contributes a relative uncertainty of 9.8×10^{-5} in the measured value of k_B . While magnetic shields can be used to reduce the field strength by a factor of 40 000 times, this was not attempted because the effect was smaller than the observed random uncertainties of the experiment.

The Rb spectra were recorded (noncontiguously) over a one-month period. While no drift would be expected from the use of a permanently sealed Rb vapor-pressure reference cell with no buffer gas, checks for long-term stability were performed by periodically reacquiring spectra at previously investigated probe power levels. We detected no long-term drift larger than the short-term reproducibility of the experiment. A long-term drift of the RL's wavelength only changes the fitted offset frequency f_0 but does not change the Rb spectrum and is therefore inconsequential.

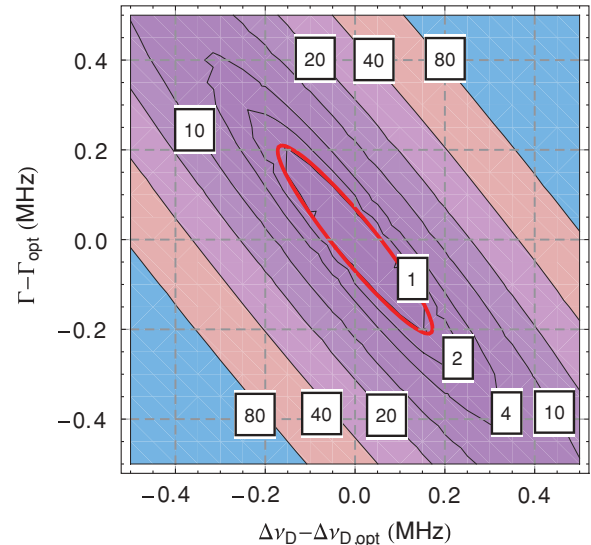


FIG. 3. (Color online) The $(\chi^2 - \chi_{\text{opt}}^2)$ surface as a function of change in Lorentzian and Gaussian widths, denoted $\Gamma - \Gamma_{\text{opt}}$ and $\Delta\nu_D - \Delta\nu_{D,\text{opt}}$, respectively, show that there is a high degree of correlation between these fit parameters. The subscripts “opt” denote the optimum quantities determined from the least-squares fit, which were 2.75 and 308.0 MHz, for the Lorentz and Gaussian widths, respectively. The thicker, red contour is generated from the covariance matrix and is intended to guide the eye.

We also considered the systematic uncertainty caused by holding Γ and S_i constant. Figure 3 demonstrates that the minimum of the χ^2 surface lies along $(\Gamma - \Gamma_{\text{opt}})/(\Delta\nu_D - \Delta\nu_{D,\text{opt}}) \approx 1$, so the propagated relative uncertainty in $\Delta\nu_D$ due to the uncertainty of Γ is reduced by a factor of $\sim \Delta\nu_D/\Gamma \approx 100$. Since the unperturbed Lorentzian width is known [23] with a relative uncertainty of 3×10^{-4} , this contributes a negligible uncertainty in $\Delta\nu_D$. Similarly, there is no uncertainty associated with the transition strengths because they are exact numbers. However, these assumptions are valid only in the limit of zero probe beam power because the measurement process itself can perturb the actual values of Γ and S_i away from their theoretical values. For example, excess probe beam power will lead to power broadening of the underlying Lorentzian linewidth, introducing an intensity dependence in the fitted Doppler width and, thus, in k_B . Similarly, any optical pumping between the hyperfine states that produces alignment or polarization of the sample will perturb the effective ratios S_i/S_j . We did, indeed, observe such effects at intensities greater than $\sim 1 \text{ W/m}^2$ (at least 30 times larger than intensities reported here), which is still more than an order of magnitude below the saturation intensity [22].

We have developed a new theory [15] to explain the cause of this early onset of optical saturation behavior, which allows us to confirm that a negligible amount of optical pumping occurred in the experiments reported here. In contrast to previous models [17,24,25] that approximate the atom as a two-level system under uniform illumination, we developed a theory for multilevel atoms probed by a beam with finite spatial extent [15]. This better captures the physical properties and situation of this Rb experiment. We find that the saturationlike behavior comes from an optical pumping process

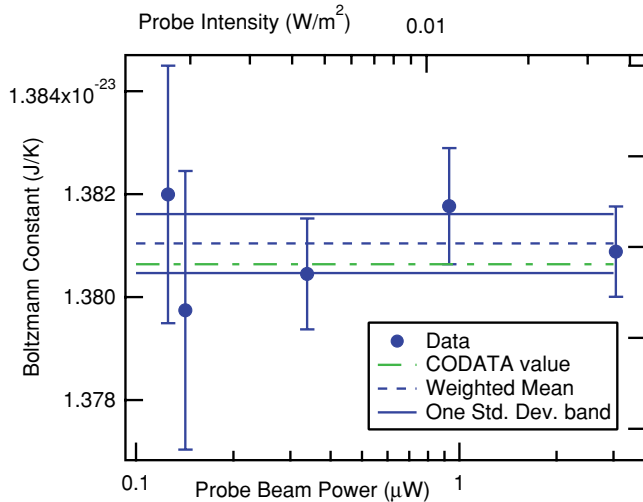


FIG. 4. (Color online) The value of k_B (dots) extracted from fitting spectra measured at several probe powers. The weighted mean (blue dashed line) and weighted one-standard-deviation band (blue solid line) are shown. The green dot-dashed line is the CODATA [6] value.

that evacuated the population in the laser-coupled ground state and not from a Rabi-oscillation mechanism responsible for saturation in a two-level system [7,26]. We therefore quantify the perturbation away from thermal equilibrium by introducing a figure of merit, denoted \mathcal{F} , defined as the relative depletion of the laser-coupled ground state, that is,

$$\mathcal{F} \equiv 1 - \frac{\rho_1}{\rho_{1,\text{th}}}, \quad (3)$$

where $\rho_{1,\text{th}}$ and ρ_1 are the thermal and pumped fractional occupation of the ground state. In the absence of optical pumping ($\rho_1 = \rho_{1,\text{th}}$), $\mathcal{F} = 0$; conversely, when the ground state is fully depleted, ($\rho_1 = 0$) and $\mathcal{F} = 1$. Using the full model of Stace and Luiten [15], we computed the figure of merit to be $\mathcal{F} \approx 0.021$ for the largest powers in this experiment. In Appendix A, we show how \mathcal{F} may be calculated approximately using a simple method based on conservation-of-energy considerations. At $\mathcal{F} = 0.021$, the perturbation in k_B due to optical pumping is 4 ppm (see Appendix B), which is well below the current statistical uncertainty. We also showed experimentally that we were sufficiently close to the zero-probe-power limit by demonstrating the absence of any statistically significant slope in the deduced value of k_B as a function of power on Fig. 4.

VI. COMPARISON TO MOLECULAR DBT

In this section, we highlight the differences between a low-pressure atomic approach and high-pressure molecular DBT experiments by examining reported results, simulated spectra, and the results presented in Sec. IV. Table II shows a comparison of some recent DBT experiments using molecules and atoms.

A. Shot-noise limits

Using the probe powers shown in Table II, row 5, we simulated shot-noise-limited Doppler-broadened spectra

TABLE II. Different experimental regimes accessed by various choices of absorbers. The relative noise reported in the bottom two rows are given for a 1000-s bandwidth.

	Rb	NH ₃ [11]	CO ₂ [12]
Doppler width (MHz)	308	50	275
Pressure (Pa)	10^{-5}	8	130
Pressure broadening (MHz)	0.02	1	4
Optical pumping, \mathcal{F}	0.021	8×10^{-8}	3×10^{-7}
Probe power (μW)	0.1	0.1	50
1000 s shot noise floor (ppm)	0.7	0.8	1.2
1000 s achieved reproducibility (ppm)	4000	1000	200

consisting of 1000 absorbance samples spanning $f_0 \pm 3\Delta\nu_D$. An approximate estimate of the shot-noise-limited relative uncertainty of k_B was found by fitting these spectra to our model. The results are surprisingly similar for all experiments (row 6). The results depend mostly on the total scan time and not details such as the frequency spacings between points. Despite the high CO₂ probe power reported in Ref. [12], the shot-noise limit is similar to the other experiments because of the low absorption depth in that experiment. The last row of Table II shows that the approximate actual repeatability calculated from reported results, when scaled to a 1000-s time scale, is significantly worse than the shot-noise limit in all cases. Djerroud *et al.* [14] have reported recent improvements to the work of Daussy *et al.* by achieving a reproducibility of 100 ppm at 1000 s. In our case, we found that background light levels have a significant impact on experimental repeatability, so we intend in future experiments to employ synchronous detection of a modulated carrier. Preliminary results suggest that this improves the repeatability to 150 ppm.

B. Optimization of probe beam power and geometry

Current approaches in DBT experiments range in pressures [12,14] from 10^{-5} to 100 Pa. In the Rb experiment described here, the mean free path is 120 m and the gas dynamics is governed by an effusive flow of atoms; that is, the system is essentially collisionless, leading to negligible pressure-induced self-broadening [7]. In contrast, the molecular DBT experiments are dominated by collisions and is in the diffusive regime, causing $\sim 0.01\Delta\nu_D$ of pressure-related broadening [11,27]. Moreover, the physical details of the molecule-molecule collisions are critical in determining the observed line-shape profile. For example, the degree of elasticity of molecular collisions perturbs the line shape away from a Voigt profile [16]. This requires higher-order forms such as the Galatry profile and a greater number of adjustable parameters required for the regression of spectra.

In contrast to the collisional effects of the molecular DBT systems the critical linewidth perturbation for vapors with strong light interaction is associated with optical pumping. This is clearly demonstrated in row 4 of Table II. To illustrate the very different operational spectroscopic regimes interrogated in this work and by Daussy *et al.* [11,14] and Casa *et al.* [12,13], Fig. 5 shows a contour plot of \mathcal{F} as a function of the nondimensional quantities Γt and $(\Omega/\Gamma)^2$. The vertical axis corresponds to the ratio of the coherent interaction time,

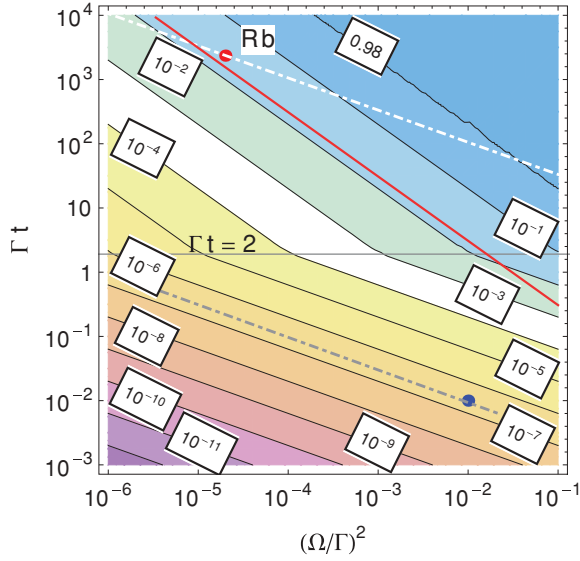


FIG. 5. (Color online) A contour plot of \mathcal{F} computed from the model of Stace and Luiten [15], as a function of normalized probe intensity $(\Omega/\Gamma)^2$ and normalized coherent evolution time (Γt) . The red and blue dots indicate the conditions of this and the molecular DBT experiments, respectively, demonstrating the exploration of vastly different spectroscopic regimes. The dot-dashed lines are contours of constant *input* power. The solid red line indicates the experimental conditions that would lead to a 1 ppm perturbation in k_B .

t , to its lifetime $(1/\Gamma)$: for an effusive vapor like Rb, t is the average beam transit time while for a diffusive gas, like those used by the molecular experiments, t is the mean time between collisions. The horizontal axis is proportional to the beam intensity and is expressed in terms of the Rabi frequency, Ω , and natural decay rate, Γ . The conventional intensity can be related to these parameters by the expression $I = 2(\Omega/\Gamma)^2 I_{\text{sat}}$, where I_{sat} is the conventional two-level saturation intensity [22]. The \mathcal{F} contours, which were calculated with the model of Stace and Luiten [15], can be closely approximated by the simpler expressions

$$\mathcal{F} \approx \begin{cases} (\Omega t/2)^2 & \text{if } \Gamma t \gg 2, \\ \Omega^2 t/(2\Gamma) & \text{if } \Gamma t \ll 2. \end{cases} \quad (4)$$

Thus, contours of constant \mathcal{F} have a slope of -1 decade versus decade and $-1/2$ decade versus decade when $\Gamma t \gg 2$ and $\Gamma t \ll 2$, respectively. Equation (4) was derived using a model of a three level atom with two ground states and an excited state. The scales of Fig. 5 obscure the details of the more complex case $\Gamma t \approx 2$, which are unimportant to this wide range overview.

In Fig. 5, the solid red line indicates the parameters where there would be a 1 ppm perturbation to the determination of k_B (derived from the analysis in Appendix B). For collisionless gases, t is proportional to the beam radius r and $(\Omega/\Gamma)^2 \propto r^{-2}$. Therefore, changing the probe beam diameter for a fixed input power leads to lines with a slope of $-1/2$ decade versus decade. Two such contours (dot-dashed) are drawn through the location of the Rb experiment reported here as well as for the molecular experiments. Contours of constant *absorbed* power follow lines of constant \mathcal{F} since the absorption coefficient is

approximately proportional to the population perturbation in the ground state; that is

$$V(f_i, \Delta\nu_D) \propto \rho_1 = \rho_{1,\text{th}}(1 - \mathcal{F}). \quad (5)$$

It is clear from Fig. 5 that there are two regimes of coherent interaction time, probe intensity, and optical pumping, which are delineated by the line $\Gamma t = 2$. For $\Gamma t \ll 2$, the contours of \mathcal{F} and those for fixed input power are parallel, demonstrating that the measured results will be independent of the probe beam geometry. However, this does not hold when $\Gamma t \gg 2$, indicating that the result will depend on probe beam shape. In this situation, Fig. 5 guides the experimenter into an optimization of probe beam radius and intensity for a given perturbation to k_B . By increasing the beam radius, it is possible to increase the *total input power* while remaining on the red line. This is advantageous as it will lead to an improved signal-to-noise ratio (SNR) of the measurement for a given linewidth perturbation. The limit to this procedure is set by the size of the gas cell. For molecular experiments where the coherent interaction time is limited by the mean time between collisions (and not the beam transit time), an increase in probe power will require a corresponding increase in pressure to preserve the amount of optical pumping. Of course, this compensation may be forgone given the much smaller magnitude of optical pumping in this regime. However, the small optical cross sections of the molecular transitions which reduce the impact of optical pumping effects give rise to other issues associated with SNR and pressure broadening.

C. Absorption depth and SNR

While Fig. 5 demonstrates the impact of experimentally controllable variables such as the coherent interaction time (which can be adjusted by changing the beam radius in an effusive gas system, and by the pressure in a diffusive gas) and the probe beam intensity, there are other considerations pertaining to the atomic-molecular properties that independently affect SNR. One such consideration is the optical depth. Numerical simulations show that in the presence of white amplitude noise (such as detector noise) there is an optimum optical depth, $\alpha L \approx 3$ at which the variance in the Doppler width obtained from repeated simulations is minimized. In terms of fundamental parameters, the optical depth can be expressed as [26]

$$\alpha L = \sigma_0 \rho_0 L \propto \Gamma \lambda^2 P L, \quad (6)$$

where σ_0 , ρ_0 , P , and L are the optical cross-section, number density, pressure of the absorber, and optical path length, respectively. We can more clearly see the trade-offs between the parameters that affect the optical depth by writing an “equation of state” for the optical depth using the conditions of the Rb experiment as the reference values,

$$\left(\frac{\alpha L}{0.7}\right) \sim \left(\frac{(\lambda \text{ in nm})^2}{780^2}\right) \left(\frac{\Gamma \text{ in s}^{-1}}{4 \times 10^7}\right) \left(\frac{P \text{ in Pa}}{3.5 \times 10^{-5}}\right) \left(\frac{L \text{ in m}}{10^{-1}}\right). \quad (7)$$

To achieve comparable SNR to atomic absorbers in which Γ is large, molecular-based approaches must compensate by increasing the product of P and L because of the much longer lifetimes. Increasing either of these parameters can lead to the potential for unwanted inaccuracies in the experiment relating to pressure broadening or thermal gradients in the apparatus.

D. Windows of operation

In this experiment, we used a commercially available Rb vapor cell of a standard length (10 cm), which gave an absorption depth of $\sim 50\%$ at room temperature. However, operating along the metal's sublimation curve means that the equilibrium vapor density increases exponentially with temperature, and thus the absorption depth is much more sensitive to temperature for atomic systems than in the molecular experiments. The range of temperatures over which we can use Rb as a thermometric substance is comparatively smaller than for molecules. The lower temperature bound is provided by the diminishing absorption depth resulting from the exponential decrease in vapor pressure. Conversely, the upper temperature bound is set when the vapor density becomes so large that the probe beam is completely absorbed over a small range of frequency detuning. Figure 6 shows approximate temperature windows over which a selection of metal gases at their vapor pressure might be able to operate [22,28–34]. At the upper and lower temperature bounds of each window, the irreproducibility of the fitted Doppler width in repeated simulations is double that for the optimal optical depth (i.e., $\alpha L \approx 3$). This condition restricts the optical depth to a range $0.5 < \alpha L < 90$. We have restricted attention to 10-cm-long cells for convenient thermal control. Some fixed points of the ITS-90 [10] scale are also shown, demonstrating that metallic vapor-pressure DBT can be used to verify the thermodynamic temperature at those fixed points.

For a particular choice of absorber, it is also possible to fill the reference cell using an external atomic reservoir at a lower temperature, resulting in a lower vapor number density. Once the vapor cell is sealed, no further increase in number

density is possible, thereby restricting optical depth to an optimum level when at high temperatures. This would permit the exploration of temperatures and pressures away from the sublimation phase boundary.

VII. CONCLUSIONS

Doppler broadening thermometry provides a significantly different approach to the determination of the Boltzmann constant in preparation for the redefinition of the kelvin. While previous DBT experiments have studied molecular absorbers at up to 10 Pa in a diffusive regime, we have used Rb at 3×10^{-5} Pa where the gas dynamics are effusive. Our approach avoids problems such as pressure broadening and poor SNR. Furthermore, the Rb cell is compact in size, enabling more convenient temperature control. We used this system to determine k_B with a relative uncertainty of 4×10^{-4} . The present experiment was limited by amplitude noise in the probe beam, which in future work will be overcome by using a control loop with larger bandwidth. We estimate that all current DBT experiments are far from the shot noise limit and that the use of synchronous detection methods could address this situation.

We also compared sources of systematic uncertainty for DBT experiments in the diffusive regime of molecular DBT and the effusive regime of atomic DBT. For atomic vapors such as Rb, the shift in the determined value of k_B due to Earth's magnetic field is approximately 100 ppm. Optical pumping effects are determined by the combination of beam transit time, upper-state lifetime and probe intensity. In this work, the equilibrium ground-state population was perturbed by 0.2%, which shifted the measured k_B value by 4 ppm. The small cross-sections of the transitions used in molecular DBT experiments mean that the optical pumping effects are relatively small (perturbation to equilibrium ground-state population of order 10^{-7}). However, these small cross-sections mean that an equivalent SNR in molecular experiments requires long path lengths and/or higher pressures, both of which have associated systematic effects on measurements of k_B . The method developed here for quantifying optical pumping effects can be used to search for candidate absorbers optimally suited to DBT experiments in either the diffusive or the effusive regimes.

APPENDIX A: APPROXIMATE METHOD FOR CALCULATING \mathcal{F}

While the approach of Stace and Luiten [15] captures the details of the gas-dynamical interaction between atoms and the beam volume, which can be used to estimate the population perturbation using no phenomenological parameters, it relies on a knowledge of the dipole matrix element in order to calculate the Rabi frequency. It is useful to compare this against a simpler, independent analytic calculation. We provide such a calculation here, based on energy conservation and using an *a posteriori* knowledge of the optical depth.

Assuming that the input intensity is sufficiently weak so that an atom never absorbs more than one photon during a single transit of the beam, the rate of atoms scattered out of

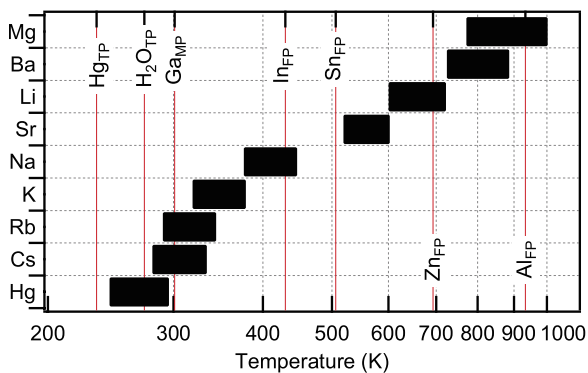


FIG. 6. (Color online) Approximate temperature windows of operation for various vapor-pressure cells, of length restricted to 10 cm. The species in each cell is shown on the vertical axis. The temperatures of selected ITS-90 fixed points are indicated by the solid vertical red lines. The subscripts TP, MP, and FP denote triple point, melting point, and freezing point, respectively.

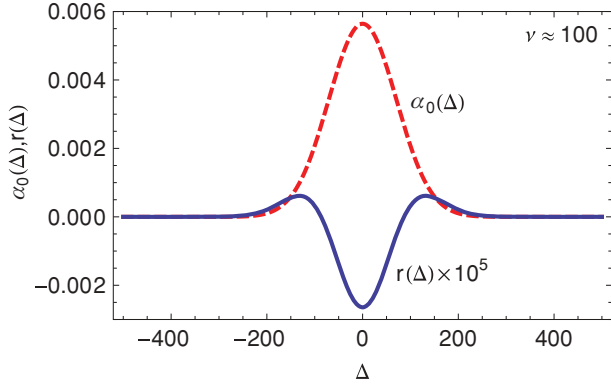


FIG. 7. (Color online) An example of the unperturbed absorption coefficient $[\alpha_0(\Delta)]$ and the additive perturbation term $[r(\Delta)]$, plotted for $\nu \approx 30 \text{ MHz}/3 \text{ MHz} = 100$. The perturbation term is vertically expanded by 10^5 for clarity. Note that ν in this appendix has a different meaning than that used in the preceding sections of this paper.

the laser-coupled ground state is approximately the same as the rate of scattered photons. This is given by

$$R = a \frac{I_0}{E_\gamma} (1 - I/I_0), \quad (\text{A1})$$

where $a = \pi r^2$ is the cross-sectional area of a beam with radius r , E_γ is the photon energy, and I and I_0 are the *on resonance* output and input intensities.

Using kinetic theory [35], the flux of atoms crossing the beam surface (of area $A = 2\pi r l$, where l is the cell length) is

$$\Phi A = \frac{1}{6} \bar{v} \rho_0 \frac{\Gamma}{\Delta \nu_D} A, \quad (\text{A2})$$

where $\bar{v} = \sqrt{2kT/m}$ is the mean atomic speed and ρ_0 is the total number density. A factor of $\Gamma/\Delta \nu_D$ is used to count only those atoms which are *on resonance*.

The value of \mathcal{F} [Eq. (3) from Sec. V] is then the ratio of the rate of scattering to the rate of new atoms impinging on the beam; that is,

$$\begin{aligned} \mathcal{F} &= R/(\Phi A) \\ &= \frac{3r}{\bar{v} \rho_0 l} \frac{\Delta \nu_D}{\Gamma} \left(\frac{I_0}{E_\gamma} \right) \left(1 - \frac{I}{I_0} \right) \\ &\approx 0.022 \quad \text{for this experiment.} \end{aligned} \quad (\text{A3})$$

This approximation agrees with the more detailed analysis, differing only by 10^{-3} .

APPENDIX B: LINEWIDTH PERTURBATION

Using the approach and notation of Stace and Luiten [15], the general expression for the absorption coefficient (Eq. (22) of Ref. [15]) can be expanded [Eq. (A1)] in the case of small optical pumping. The expression for a perturbed absorption

coefficient line shape is

$$\begin{aligned} \alpha &\approx \frac{\kappa c P_1 z}{2\omega} \left[\left\{ \frac{P_3'' - P_1''}{P_1} \frac{\sqrt{\nu^2 + 1/4}}{8\nu} - \pi \right\} V(\Delta, \nu) \right. \\ &\quad \left. + \frac{P_3'' - P_1''}{P_1} \frac{4(\Delta/\nu)^2 - 3}{64\sqrt{\pi}\nu^3} \exp\left(-\frac{\Delta^2}{\nu^2 + 1/4}\right) \right] \\ &\approx \alpha_0(\Delta) + \epsilon r(\Delta), \end{aligned} \quad (\text{B1})$$

where $\alpha_0(\Delta)$ is the unperturbed line shape, $r(\Delta)$ is defined as the exponential term in the parentheses, and Δ is the detuning in units of the Gaussian width. Figure 7 shows a plot of the unperturbed line shape along with the perturbation term $r(\Delta)$. We performed an expansion in the small parameter $\epsilon \equiv (P_3'' - P_1'')/P_1$, where $P_i'' \equiv \partial^2 P_i / \partial \Delta^2$ the derivative is with respect to the detuning Δ . The meanings of the remaining variables in this section are as defined in Ref. [15]. Written in this form, it is clear that the absorption coefficient in the presence of some optical pumping is a Voigt function, denoted $V(\Delta, \nu)$ with an additional perturbation term.

Consider the expansion of a characteristic width for the perturbed absorption coefficient,

$$\Delta_{1/e, \text{pert}}(\epsilon) \approx \Delta_{1/e, \text{pert}}(0) + \left. \frac{d\Delta_{1/e, \text{pert}}}{d\epsilon} \right|_{\epsilon=0} \delta\epsilon, \quad (\text{B2})$$

such that $\alpha(\Delta_{1/e, \text{pert}})/\alpha(0) \equiv 1/e$. Differentiating this definition and using $\Delta_{1/e, \text{pert}}(0) = \Delta_{1/e}$, we obtain the perturbation to the linewidth

$$\begin{aligned} \left. \frac{d\Delta_{1/e, \text{pert}}}{d\epsilon} \right|_{\epsilon=0} &= \frac{\alpha_0(0)[r(0)/e - r(\Delta_{1/e})]}{[\alpha_0(0) + \epsilon r(0)][\alpha_0'(\Delta_{1/e}) + \epsilon r'(\Delta_{1/e})]} \\ &\approx \frac{a_0(0)[r(0)/e - r(\Delta_{1/e})]}{a_0 a_0'(\Delta_{1/e})} \\ &\approx -\frac{1/e}{16\sqrt{\pi}\nu^3} \frac{1}{\alpha_0'(\Delta_{1/e})} \\ &\approx -\frac{1}{32\sqrt{\pi}\nu^2}. \end{aligned} \quad (\text{B3})$$

To evaluate $\delta\epsilon$, we have used the low-probe-power approximation of Stace and Luiten ($P_3 \approx 0 \ll P_1$) and $\Delta_{1/e} \approx \nu \equiv \Delta \nu_D / \Gamma \approx 100 \gg 1$. We also used the approximate form for the steady-state population density P_1 that ignores atomic coherence. This quantity is maximal on resonance (i.e., when $\Delta = 0$):

$$\begin{aligned} \text{Max}[P_1''] &= P_1''(0) = \frac{d^2}{d\Delta^2} \left\{ \frac{1}{2} \left[1 - \exp\left(-\frac{\Omega^{*2} t^*}{1 + 4\Delta^{*2}}\right) \right] \right\} \Big|_{\Delta=0} \\ &= -4t^* \Omega^{*2} \exp(-t^* \Omega^{*2}) \\ &< -4t^* \Omega^{*2} \\ &\approx -0.4 \quad \text{for this experiment.} \end{aligned}$$

Substitution of the relevant quantities into Eq. (B2) gives 2 ppm perturbation to the linewidth and, therefore, 4 ppm in the determination of k_B for this experiment.

[1] H. Preston-Thomas, *Metrologia* **27**, 3 (1990).

[2] L. Pitre, M. R. Moldover, and W. L. Tew, *Metrologia* **43**, 142 (2006).

[3] Consultative committee for thermometry recommendation T2 (2005) to the CIPM [www.bipm.org/cc/CCT/Allowed/23/CCT_05_31.pdf].

- [4] B.-Fellmuth, C. Gaiser, and J. Fischer, *Meas. Sci. Technol.* **17**, R145 (2006).
- [5] I. M. Mills, P. J. Mohr, T. J. Quinn, B. N. Taylor, and E. R. Williams, *Metrologia* **43**, 227 (2006).
- [6] M. R. Moldover, J. P. M. Trusler, T. J. Edwards, J. B. Mehl, and R. S. Davis, *Phys. Rev. Lett.* **60**, 249 (1988).
- [7] W. Demtröder, *Laser Spectroscopy* (Springer, Berlin, 1981).
- [8] A. Unsöld and B. Baschek, *The New Cosmos: An Introduction to Astronomy and Astrophysics* (Springer Verlag, Berlin, 2001).
- [9] C. J. Bordé, *Philos. Trans. R. Soc. London A* **363**, 2177 (2005).
- [10] J. Fischer and B. Fellmuth, *Rep. Prog. Phys.* **68**, 1043 (2005).
- [11] C. Daussy, M. Guinet, A. Amy-Klein, K. Djerroud, Y. Hermier, S. Briaudeau, C. J. Bordé, and C. Chardonnet, *Phys. Rev. Lett.* **98**, 250801 (2007).
- [12] G. Casa, A. Castrillo, G. Galzerano, R. Wehr, A. Merlone, D. Di Serafino, P. Laporta, and L. Gianfrani, *Phys. Rev. Lett.* **100**, 200801 (2008).
- [13] A. Castrillo, G. Casa, A. Merlone, G. Galzerano, P. Laporta, and L. Gianfrani, *C. R. Phys.* **10**, 894 (2009).
- [14] K. Djerroud *et al.*, *C. R. Phys.* **10**, 883 (2009).
- [15] T. M. Stace and A. N. Luiten, *Phys. Rev. A* **81**, 033848 (2010).
- [16] B. Wende, ed., *Spectral Line Shapes: Proceedings 5th International Conference* (Walter de Gruyter, Berlin, 1981).
- [17] D. J. Shin, *Metrologia* **42**, 154 (2005).
- [18] E. D. Black, *Am. J. Phys.* **69**, 79 (2001).
- [19] M. P. Bradley, J. V. Porto, S. Rainville, J. K. Thompson, and D. E. Pritchard, *Phys. Rev. Lett.* **83**, 79 (1999).
- [20] E. Arimondo, M. Inguscio, and P. Violino, *Rev. Mod. Phys.* **49**, 31 (1977).
- [21] J. Humlíček, *J. Quant. Spectrosc. Radiat. Transfer* **27**, 437 (1982).
- [22] D. A. Steck, Rubidium-85 d line data. 2008 Available online [<http://george.ph.utexas.edu/~dsteck/alkalidata/index.html>].
- [23] J.-E. Simsarian, L. A. Orozco, G. D. Sprouse, and W. Z. Zhao, *Phys. Rev. A* **57**, 2448 (1998).
- [24] M. L. Harris, C. S. Adams, S. L. Cornish, I. C. McLeod, E. Tarleton, and I. G. Hughes, *Phys. Rev. A* **73**, 062509 (2006).
- [25] P. Siddons, C. S. Adams, C. Ge, and I. G. Hughes, *J. Phys. B* **41**, 155004 (2008).
- [26] A. E. Siegman, *Lasers* (University Science Books, Mill Valley, CA, 1986).
- [27] T. Le Barbu, B. Parvitte, V. Zéninari, I. Vinogradov, O. Korablev, and G. Durry, *Appl. Phys. B* **82**, 133 (2006).
- [28] D. R. Lide, ed., *CRC Handbook of Chemistry and Physics* (CRC Press, Boca Raton, FL, 1993).
- [29] N. B. Pilling, *Phys. Rev.* **18**, 362 (1921).
- [30] E. Rudberg and J. Lempert, *J. Chem. Phys.* **3**, 627 (1935).
- [31] W. P. Gilbreath, *The Vapor Pressure of Magnesium Between 223 and 385 C*, NASA Technical Reports (1965).
- [32] M. L. Huber, A. Laesecke, and D. G. Friend, *The Vapor Pressure of Mercury*, NIST Interagency Reports (2006).
- [33] X. Xu, T. H. Loftus, J. L. Hall, and A. Gallagher, *JOSA B* **20**, 968 (2003).
- [34] M. Asano and K. Kubo, *J. Nucl. Sci. Technol.* **15**(10), 765 (1978).
- [35] F. Reif, *Fundamentals of Statistical and Thermal Physics* (McGraw-Hill, New York, 1965).